CENTRE FOR **STOCHASTIC GEOMETRY**
AND ADVANCED **BIOIMAGING**

Nick Yin Larsen, Johanna F. Ziegel, Jens R. Nyengaard
and Eva B. Vedel Jensen

Stereological estimation of particle shape from vertical sections

No. 12, December 2018

Stereological estimation of particle shape from vertical sections

Nick Yin Larsen[1,2,3], Johanna F. Ziegel[1,4], Jens R. Nyengaard[1,2,3] and Eva B. Vedel Jensen[1,5]

[1]Centre for Stochastic Geometry and Advanced Bioimaging, Aarhus University
[2]Core Centre for Molecular Morphology, Section for Stereology and Microscopy, Department of Clinical Medicine, Aarhus University
[3]Sino-Danish Center for Education and Research (SDC)
[4]Institute of Mathematical Statistics and Actuarial Science, University of Bern
[5]Department of Mathematics, Aarhus University

Summary

In the present paper, we describe a new simple stereological method of estimating volume tensors in 3D from vertical sections. The volume tensors provide information about particle shape in 3D. In a model-based setting, the method requires that the particle distribution is invariant under rotations around the vertical axis. In a design-based approach, where the vertical section is uniformly rotated around the vertical axis, the method provides information about an index of elongation of the particles in the direction of the vertical axis. The method has been implemented on human brain tissue for the analysis of neurons in layer III of the medial frontal gyrus of Brodmann Area 46. In the actual implementation, the new estimator shows similar precision as an earlier estimator, based on an optical rotator design, but it is a factor 3 faster to collect the measurements for the new estimator.

1 Introduction

Recently, stereological methods of estimating particle shape in 3D have been developed for arbitrarily shaped particles ([13], [20]). The methods use volume tensors of rank 0, 1 and 2, from which ellipsoidal approximations to the particles can be constructed. Earlier methods provided information about shape of 2D particle sections ([2], [3], [4], [19]). In particular, 2D analogues of volume tensors were used to describe shape of cell sections ([2], [3], [4]).

In [13] and [20], the volume tensors in 3D are estimated from observations in several optical planes through a sample of particles. The design is called the optical rotator and has earlier been used for estimating particle volume and surface area ([18]).

As shown in the recent book chapter [12], a much simpler alternative method, which is a generalization of the planar vertical rotator ([10]), can be constructed. This method uses measurements in a single optical plane, passing through a reference point of each sampled particle.

The purpose of our paper is to present this new and simple method to scientists working in optical light microscopy. In a model-based setting, the method requires that the particle distribution is invariant under rotations around the vertical axis. In a design-based approach where the vertical section is uniformly rotated around the vertical axis, the method provides information about an index of elongation of the particles in the direction of the vertical axis.

The method has been implemented on human brain tissue for the analysis of neurons in layer III of the medial frontal gyrus of Brodmann Area 46. This area was chosen, since it has been the subject of studies related to schizophrenia and depression ([1], [5], [6], [7], [11], [16]). Methods of assessing the precision of the new estimator, based on a bootstrap procedure, are also provided.

The paper is organized as follows. First, we introduce the volume tensors. Then, we discuss inference for particle populations and show how the mean particle volume tensors can be estimated, using the planar vertical rotator design. Finally, volume tensor data collected on neurons from a human brain in layer III of the medial frontal gyrus of Brodmann Area 46 are analyzed. Data, using the planar rotator as well as the optical rotator, are available on the same set of neurons. Finally, we discuss our results and further research questions. Some derivations are deferred to two Appendices.

2 Volume tensors

In this section, we introduce the volume tensors in $\mathbb{R}^3$ and show how they can be used for obtaining information about size, position, shape and orientation of a spatial particle.

Let k be a non-negative integer. The volume tensor of rank k associated with a particle X (compact subset of $\mathbb{R}^3$) is given by

$$T_k(X) = \frac{1}{k!} \int_X u^k \, \mathrm{d}u, \tag{1}$$

where u^k is the symmetric tensor of rank k, determined by $u = (u_1, u_2, u_3) \in \mathbb{R}^3$, and the integration is with respect to volume (Lebesgue) measure in $\mathbb{R}^3$. Here, $u^0 = 1$ and $u^1 = u$, while u^2 is the symmetric 3×3 matrix with elements $(u^2)_{i,j} = u_i u_j$, $i, j = 1, 2, 3$. For general k, the tensor u^k can be represented as a k-dimensional array. The integration in (1) is to be understood elementwise.

We will focus on volume tensors of rank 0, 1 and 2. The volume tensor of rank 0

$$T_0(X) = \int_X 1 \, \mathrm{d}u = V(X)$$

is simply the volume of X, while the volume tensor of rank 1 is the following point in $\mathbb{R}^3$

$$T_1(X) = \left(\int_X u_1 \, \mathrm{d}u, \int_X u_2 \, \mathrm{d}u, \int_X u_3 \, \mathrm{d}u \right).$$

It follows that $T_1(X)/T_0(X)$ is the centre of gravity $c(X)$ of X, indicating the *position* of X in $\mathbb{R}^3$. The volume tensor of rank 2 can be represented as a 3×3 matrix with (i, j)'th entry

$$T_2(X)_{i,j} = \frac{1}{2} \int_X u_i u_j \, \mathrm{d}u, \qquad i, j = 1, 2, 3.$$

Combining $T_0(X)$, $T_1(X)$ and $T_2(X)$, we can obtain information about the *shape* and *orientation* of X. Thus, these tensors can be used to construct a centred ellipsoid $e(X)$ of the same volume as X such that $c(X)+e(X)$ is an ellipsoidal approximation to X, cf. Figure 1. If X is an ellipsoid, then $X = c(X) + e(X)$. The ellipsoid $e(X)$ can be determined from a spectral decomposition of $T_2(X - c(X))$,

$$T_2(X - c(X)) = T_2(X) - \frac{T_1(X)^2}{2T_0(X)} = B\Lambda B^T,$$

where B is an orthogonal matrix and Λ is a diagonal matrix with diagonal elements λ_i, $i = 1, 2, 3$. The ellipsoid $e(X)$ is determined by having directions of semi-axes equal to the columns of B, lengths of semi-axes proportional to $\sqrt{\lambda_i}$, $i = 1, 2, 3$, and volume equal to $V(X)$.

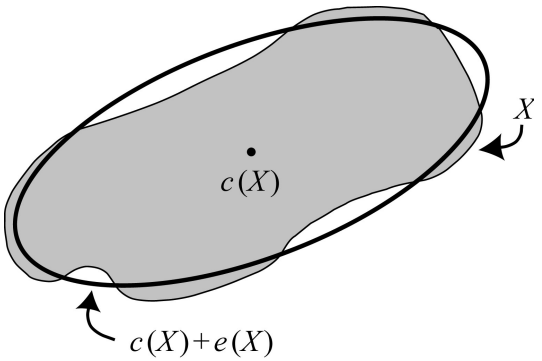

Figure 1: 2D illustration of the ellipsoidal approximation to a particle X (light grey). Here, $c(X)$ is the centre of gravity of X and $e(X)$ is a centred ellipsoid, approximating $X - c(X)$. If X is an ellipsoid, $X = c(X) + e(X)$.

3 Inference for particle populations

In the present paper, we are interested in making inference for a particle population at the population level. Parameters of interest are, for instance, mean particle volume and mean particle shape.

We will assume that we can associate a reference point $x_i \in X_i$ to each particle X_i. We let $\bar{T}_k$, $k = 0, 1, 2$, be the mean particle volume tensor of rank k, where each particle X_i enters in the mean with its own reference point x_i as origin. For $k = 0$, we get the mean particle volume $\bar{v} = \bar{T}_0$, while $\bar{c} = \bar{T}_1/\bar{T}_0$ is the so-called *displacement vector* ([13, p. 232]), containing information about the average difference between the centre of gravity and the reference point of the particles in the population. See Figure 2 for an illustration.

Furthermore, a centred ellipsoid $\bar{e}$ can be constructed that provides information about average particle shape and orientation. The ellipsoid $\bar{e}$ is called the *Miles ellipsoid* after Roger Miles who was a pioneer in the development of stereological methods for particle populations with arbitrarily shaped particles. The Miles ellipsoid is determined from $\bar{T}_0$, $\bar{T}_1$ and $\bar{T}_2$, using exactly the same method as the one used for determining $e(X)$ from $T_0(X)$, $T_1(X)$ and $T_2(X)$. If the particles X_i are translations of the same particle X_0, then the Miles ellipsoid is simply the approximating ellipsoid $e(X_0)$. The concept of the Miles ellipsoid is also illustrated in Figure 2. Further illustrations of the displacement vector and the Miles ellipsoid may be found in [13, Fig. 3].

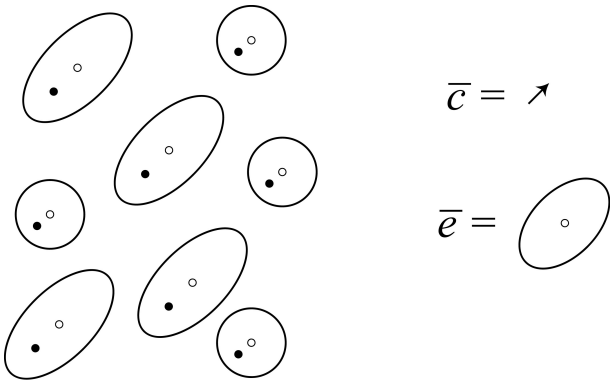

Figure 2: 2D illustration of the displacement vector $\bar{c}$ and the Miles ellipsoid $\bar{e}$ for a particle population, consisting of an equal mixture of ellipses and circular disks. The centre of gravity of a particle is indicated by an open circle and the reference point by a closed circle.

The estimates of the mean particle volume tensors will be based on a random sample of particles. One possibility is to sample all particles with reference point in a 3D sampling window W. The indices of the sampled particles are then

$$S = \{i : x_i \in W\}.$$

In the case of disector sampling ([17]), W may be a set of systematically placed sampling boxes. An estimator of $\bar{T}_k$ is the following

$$\frac{1}{N(W)} \sum_{i \in S} T_k(X_i - x_i), \tag{2}$$

$k = 0, 1, 2$, where $N(W)$ is the number of sampled particles.The estimator (2) is ratio-unbiased if W has a uniform random position (design-based approach) or the particles can be modelled by a stationary point process model (model-based approach, see Appendix A).

However, for the determination of the estimator (2), we need to be able to determine the volume tensors T_k directly on the sampled spatial particles. For the case where we do not have direct access to the particles in 3D, an estimator of T_k based on observation in an optical rotator, consisting of several optical planes, has been developed in [13]. As we shall see in the next section, a much simpler alternative method can be constructed based on observations in a planar vertical rotator.

4 Estimation using the planar vertical rotator

In this section, we present an estimator of $\bar{T}_k$ that only uses measurements in vertical planes passing through the reference points of the sampled particles.

The estimator is valid in a model-based setting if the particles can be modelled by a stationary marked point process, satisfying the assumption of rotational invariance with respect to a predetermined fixed axis, called the vertical axis. (We use this terminology for the axis also in cases where it is not vertical.) The particle process is rotation invariant, if the particle distribution is invariant under rotations around the vertical axis. Under rotational invariance, the vertical axis represents the average orientation of the particles in 3D and, as we shall see, the mean particle shape in 3D can be estimated from observations in vertical planes. The point process model is described in detail in Appendix A where also rotational invariance is formally defined.

The design used for each sampled particle X is a new, innovative application of the planar vertical rotator design ([10]), involving registration of 3D coordinates of intersection points. The design consists of a plane, passing through the reference point of the particle, taken here to be the origin O. The plane contains the vertical axis. The section is subsampled by a systematic set of alternating half lines, perpendicular to the vertical axis, see Figure 3.

In [12, p. 427-429], ratio-unbiased estimators of $\bar{T}_k$ are derived under the rotational invariance assumption. (In [12], 'rotational invariance' was called 'restricted isotropy'.) The estimators $\widehat{T}_k$ are of the following form

$$\widehat{T}_k = \frac{1}{N(W)} \sum_{i \in S} \widetilde{T}_k([X_i - x_i] \cap L), \tag{3}$$

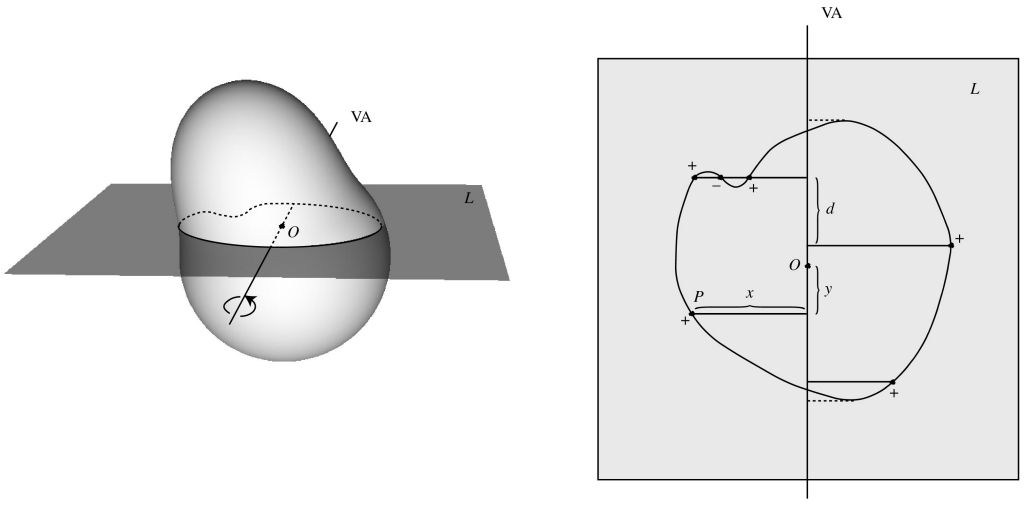

Figure 3: (Left) The particle X is sectioned by a vertical plane, containing the vertical axis (VA) and passing through the reference point O of the particle. (Right) The section is subsampled by a systematic set of half lines. The intersection points on a given half line are ordered according to decreasing distance to VA and are given alternating signs, starting with + for the most distant intersection point.

where L is the notation used for the vertical plane. The ratio-unbiasedness relies on the fact that under rotational invariance the distribution of size, orientation and shape of the section profiles $\{[X_i - x_i] \cap L\}$ does not depend on the rotation of L around the vertical axis. An illustration of this property may be found in [9, Fig. 10].

In Appendix A, the explicit form of $\widetilde{T}_k$ is derived for $k = 0, 1, 2$. For a sampled particle X with reference point O, $\widetilde{T}_k(X \cap L)$ is a sum over intersection points $\{P_j\}$ between half lines and the boundary of X

$$\widetilde{T}_k(X \cap L) = \sum_j^{+/-} g_k(P_j), \qquad k = 0, 1, 2. \tag{4}$$

The sign of an intersection point is also shown in Figure 3. If we let d be the distance between neighbour half lines and choose a coordinate system such that L is the xy-plane and the vertical axis is the y-axis, then we get for an intersection point $P = (x, y, 0)$

$$g_0(x, y, 0) = \pi d\, x^2, \tag{5}$$

$$g_1(x, y, 0) = (0, \pi d\, x^2 y, 0), \tag{6}$$

$$g_2(x, y, 0) = \begin{pmatrix} \frac{\pi}{8} d\, x^4 & 0 & 0 \\ 0 & \frac{\pi}{2} d\, x^2 y^2 & 0 \\ 0 & 0 & \frac{\pi}{8} d\, x^4 \end{pmatrix}. \tag{7}$$

The estimator of volume obtained by using the g_0-function already appeared in [10]. Note that the g_k-functions, $k = 0, 1, 2$, are much simpler than the ones appearing in [13, p. 231] where the optical rotator was used instead of the planar vertical rotator.

Under the assumption of rotational invariance, the mean particle volume is estimated by $\widehat{v} = \widehat{T}_0$ and the displacement vector by $\widehat{c} = \widehat{T}_1/\widehat{T}_0$. An estimator $\widehat{e}$ of the Miles ellipsoid can be calculated from $\widehat{T}_0$, $\widehat{T}_1$ and $\widehat{T}_2$, using the same procedure as the one used for constructing $e(X)$ from $T_0(X)$, $T_1(X)$ and $T_2(X)$.

Note that the estimated displacement vector $\widehat{c}$ is parallel to the vertical axis. Furthermore, the estimated Miles ellipsoid $\widehat{e}$ is an ellipsoid of revolution around the vertical axis, since

$$\widehat{T}_2 - \frac{(\widehat{T}_1)^2}{2\widehat{T}_0}$$

is a diagonal matrix with first and third diagonal elements equal. Under rotational invariance, the same is true for the theoretical quantities $\bar{c}$ and $\bar{e}$, see Appendix A.

5 Relaxing the rotational invariance assumption

When rotational invariance is satisfied, it is not needed to rotate the vertical planes around the vertical axis. However, if rotational invariance is not a plausible model assumption, one may instead adopt a design-based approach and use vertical planes that are uniformly rotated around the vertical axis. More specifically, rotational invariance may be introduced into the model by letting the vertical plane L, used in the estimators $\widehat{T}_k$ in (3), have a uniform rotation around the vertical axis. An

equivalent description of the situation is that each centred particle $X_i - x_i$ is given a random rotation and then sectioned by a fixed vertical plane L_0, say. The induced particle model satisfies the rotational invariance assumption.

Under this design-based approach, $\widehat{v}$ is still an unbiased estimator of the mean particle volume $\bar{v}$. As explained in Appendix A, $\widehat{c}$ becomes an estimator of the projection onto the vertical axis of the displacement vector $\bar{c}$.

In this design-based approach, the estimator $\widehat{e}$ of the Miles ellipsoid may be used to estimate an index I of elongation of the particles in the direction of the vertical axis. The Miles ellipsoid in the induced model is an ellipsoid of revolution around the vertical axis. If the lengths of the semi-axes of this ellipsoid, parallel and perpendicular to the vertical axis, are denoted a and b, respectively, then the elongation index I is

$$I = a/b.$$

Large values of I indicate elongation in the direction of the vertical axis. The index I takes the value 1, if the original particle population is isotropic. More details about this index may be found in Appendix A.

6 Practical implementation of tensors in optical light microscopy

In this section and the next, we exemplify the estimation of volume tensors, using the planar vertical rotator design, as explained in the previous sections. The resulting estimator (3) of the volume tensor of rank k will here be called *the section estimator*. We will compare the performance of the section estimator with that of the estimator developed in [13], based on the optical rotator design. The latter estimator will be called *the slice estimator*.

The two types of volume tensor estimation methods were used on the same set of neurons from a 40 µm thick section from layer III of the medial frontal gyrus (MFG) of Brodmann Area 46 (BA46) in the human cerebral cortex ([14], [15]). One formalin-fixed brain from a male patient with no history of neurological condition was selected from the brain collection at Core Centre for Molecular Morphology, Section for Stereology and Microscopy, Aarhus University Hospital, Aarhus, Denmark. The brain was collected in accordance with Danish law and with permission from the local ethical committee, see case no. 1-10-72-91-17. Data were obtained, using an Olympus BX51 light microscope with Olympus DP70 camera, an Olympus 60x oil lens (NA=1.35), prior motorized stage and newCAST software (Visiopharm, Hørsholm, Denmark).

The sampling of tissue is illustrated in Figure 4 while the sample area within MFG used for further analysis is marked as a yellow rectangle in Figure 5. The sample area was analyzed with a systematic set of disectors, resulting in 111 sampled neurons. The nucleolus of a neuron was used as reference point in the sampling. Figure 6 illustrates the collection of measurements for a sampled neuron, required for the section estimator. In the actual implementation, $n = 4$ half lines were used. An illustration of the measurements required for the slice estimator may be found in [13, Fig. 7]. Three optical planes were used for analysis of a sampled neuron and

each optical plane was analyzed by two full lines. Since the expected number of intersection points is three times larger for the slice estimator than for the section estimator, the expected workload associated with the slice estimator is three times larger than that of the section estimator.

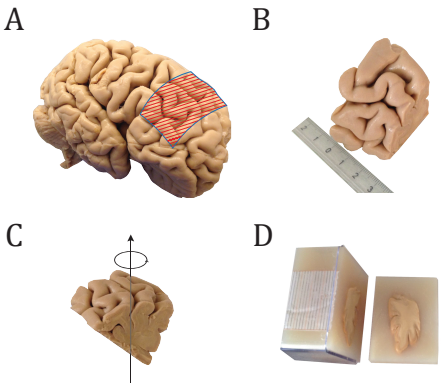

Figure 4: (A) The region BA46 is defined by its cytoarchitecture and is part of the Dorsolateral Prefrontal Cortex (DLPFC) which can be identified at the macroscopic level. (B) A coronal block of DLPFC. (C) The tissue block is rotated uniformly around a vertical axis (VA), perpendicular to the central pial surface of the block. (D) After agar hardening, the block is cut into 2.5 mm thick parallel vertical slabs. The slabs are embedded in plastic (Technovit 7100) and subsequently cut into 40 µm thick sections that are stained with a Toluidinblue-Borax solution before further analysis.

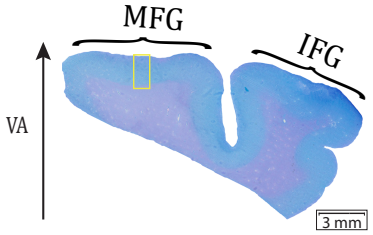

Figure 5: The sample area within the medial frontal gyrus (MFG) is marked with a yellow rectangle. The inferior frontal gyrus (IFG) is also indicated. VA is the vertical axis.

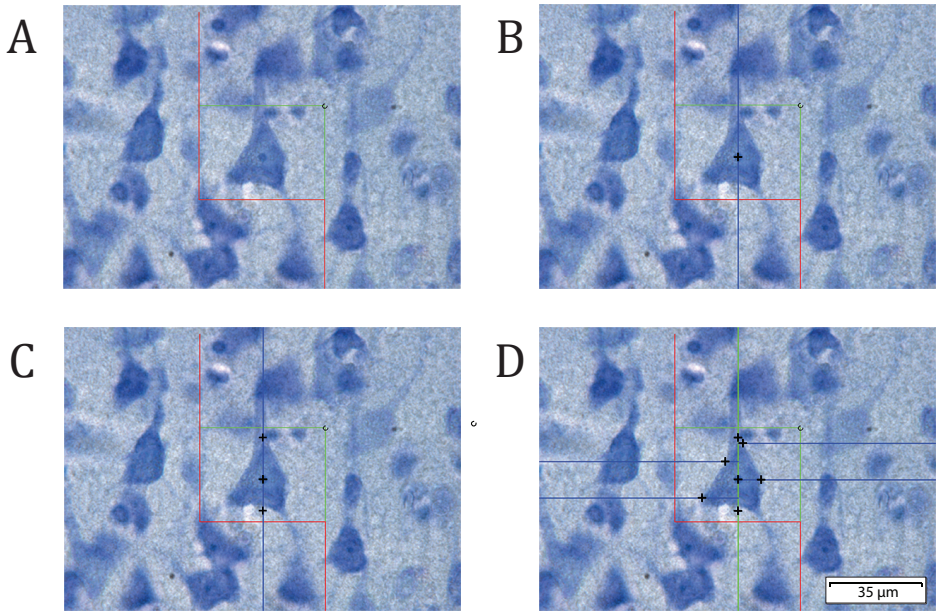

Figure 6: Measurement steps for a sampled neuron in layer III of the medial frontal gyrus in BA46, required for the section estimator. (A) A neuron in focus inside the optical disector. (B) The nucleolus was chosen as the reference point and the pre-defined vertical axis appears as a blue line. (C) The cell boundary in the vertical direction (top and bottom) are marked. (D) Four half lines perpendicular to the vertical axis with uniform random position appear. The intersection points between the neuron boundary and the half lines are marked with +.

7 Tensor data analysis

In Table 1, we show the estimated mean particle volume $\widehat{v}$, the signed length of the estimated displacement vector $\widehat{c}$, the lengths of the semi-axes of the estimated Miles ellipsoid $\widehat{e}$ and the estimated elongation index, based on the section and the slice estimators, respectively. Recall that the elongation index is the ratio between the lengths of the semi-axes parallel and perpendicular to the vertical axis. Since we have taken a design-based approach and rotated the tissue block uniformly around the vertical axis, we do not need to assume rotational invariance and, in this case, $\widehat{c}$ estimates the average distance along the vertical axis from the nucleolus to the centre of gravity of a neuron. Likewise, as explained earlier, the estimate of the elongation index is valid without rotational invariance.

The estimated mean particle volumes, based on the section and the slice estimator, are quite similar and in fact equal to volumes of balls of radii 10.77 µm and 10.99 µm, respectively. As a further investigation, we plot in Figure 7 the estimated particle volume, based on the slice estimator, against the estimated particle volume, based on the section estimator, for each of the 111 sampled neurons separately.

It is of course important to know the precision of the estimates, presented in Table 1. The variance of the volume estimators $\widehat{v}$ can be estimated by the empirical variance. The displacement vector is estimated by a ratio so, using a Taylor

Table 1: For the sample of 111 neurons, the table shows the estimated mean particle volume, the signed length of the estimated displacement vector, the lengths of the semi-axes of the estimated Miles ellipsoid and the estimated elongation index, based on the section and the slice estimators, respectively. For more details, see the text.

	Section estimator	Slice estimator
Volume (µm^3)	5235	5558
Displacement (µm)	1.86	2.00
Parallel semi-axis (µm)	12.77	13.85
Perpendicular semi-axes (µm)	9.89	9.79
Elongation index	1.29	1.41

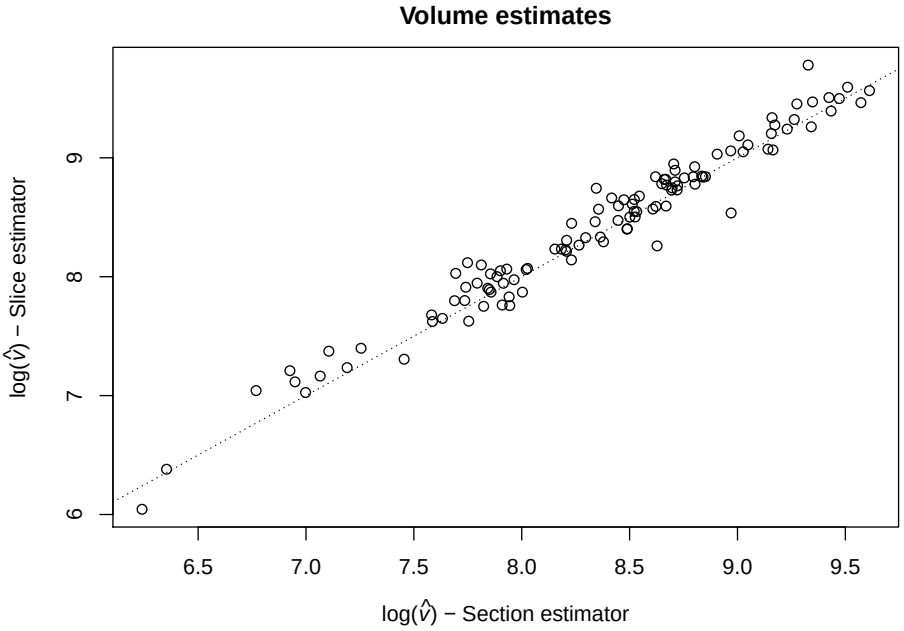

Figure 7: For each of the 111 sampled neurons, the volume estimate, based on the slice estimator, is plotted against the volume estimate, based on the section estimator. The dotted line is the identity.

expansion of the ratio combined with empirical variances/covariances, we can obtain an estimate of the variance of the signed length of the displacement estimator. Estimation of the variances of the quantities relating to the Miles ellipsoid is more complicated. However, for any of the estimators, we can use classical resampling bootstrap to assess the variance, assuming that our sample is at least approximately independent and identically distributed ([8]). The results are given in Table 2. The alternative variance estimation methods mentioned above gave similar results, when applicable.

Part of the variance of the section estimator is due to the random positioning of the half lines on the neuron profiles. For the slice estimator, the random positioning of the three optical planes and the lines within the optical planes contribute to the variance. In order to assess the magnitude of this design variance in relation to

Table 2: Estimated bias and coefficient of variation for the sample of 111 neurons. Since the displacement vector may have zero length, the standard deviation is reported instead of the coefficient of variation for this parameter. For more details, see the text.

		Section estimator	Slice estimator
		Bootstrap	Bootstrap
Volume	CV	0.059	0.060
Displacement	Bias	−0.003	−0.001
	SD	0.309	0.289
Parallel	Bias	0.004	0.002
semi-axis	CV	0.027	0.039
Perpendicular	Bias	−0.006	−0.002
semi-axes	CV	0.026	0.027
Elongation	Bias	0.002	0.002
index	CV	0.035	0.051

the total estimator variance, we performed 5 repeated measurements of 20 sampled neurons. Since the sampled neurons come from the same vertical slab, the remaining part of the total estimator variance includes variability due to the rotation of the slab around the vertical axis.

We will focus on estimation of mean particle volume, displacement and elongation index. The obtained estimates based on all data are shown in Table 3, together with the average time spent collecting a single set of measurements on one sampled neuron. Note that the estimated mean particle volumes, based on the section and the slice estimator, equal volumes of balls of radii 11.4 µm and 11.7 µm, respectively. Note also that the time is approximately a factor 3 larger for the slice estimator than for the section estimator.

In Tables 4–6, we assess the precision of the estimator of volume, displacement and elongation index in the case when a single set of measurements is available for 20 neurons. A bootstrap procedure can be used for this assessment, see Appendix B.

Table 3: The table shows for the section and the slice estimators, respectively, the estimated mean particle volume, the signed length of the estimated displacement vector and the estimated elongation index, based on 5 repeated measurements of 20 sampled neurons. The average time spent collecting a single set of measurements on one sampled neuron is also shown.

	Section estimator	Slice estimator
Volume (µm^3)	6151	6747
Displacement (µm)	0.41	0.078
Elongation index	1.198	1.257
Time (s)	7.0	19.5

In Table 4, we show the components of the estimated variance for the mean particle volume estimator. The variance estimates have been determined empirically and by a bootstrap procedure, see Appendix B. When using bootstrap, the total variance may either be estimated as the sum of the average design variance and the particle variance (indicated by (+) in Table 4) or by a separate procedure. Note that the obtained coefficient of variation (CV) is 17% for both the section and the slice estimator. This is the precision of the estimated mean particle volume, when using a single set of measurements on 20 neurons.

Table 4: Components of the variance for volume estimators. For more details, see the text.

	Section estimator		Slice estimator	
	Empirical	Bootstrap	Empirical	Bootstrap
Average design variance	12836	10291	76125	60149
Particle variance	1056755	1005402	1226403	1165501
Total variance	1069590	(+)1015693	1302528	(+)1225650
		1027098		1230964
Total CV	0.168	0.165	0.169	0.164

The components of the estimated variance of the displacement estimator, based on a single set of measurements on 20 neurons, may be found in Table 5. An estimate of the bias of the estimator of the signed length of the displacement may also be found in Table 5. As explained in Appendix B, the variance components may in the case of the section estimator be estimated, using a Taylor expansion or a bootstrap method. The estimated bias is small in absolute terms.

Table 5: Bias, variance and SD for the signed length of the displacement. For more details, see the text.

	Section estimator		Slice estimator
	Taylor	Bootstrap	Bootstrap
Bias	—	0.047	0.017
Average design variance	0.050	0.093	0.100
Particle variance	0.941	0.877	0.719
Total variance	0.991	(+)0.970	(+)0.820
	—	0.967	0.817
Total SD	0.995	0.983	0.904

In Table 6, the results for the elongation index are shown. The estimated bias is again small in absolute terms.

In Tables 4–6, the section and the slice estimator show similar performance, regarding bias and variance. However, the time spent for determining the slice estimator is a factor 3 longer than for the section estimator.

Table 6: Bias, variance and CV for the elongation index. For more details, see the text.

	Section estimator	Slice estimator
	Bootstrap	Bootstrap
Bias	0.0260	0.0044
Average design variance	0.0037	0.0035
Particle variance	0.0161	0.0060
Total variance	(+)0.0198	(+)0.0095
	0.0193	0.0095
Total CV	0.1160	0.0775

8 Discussion

In the present paper, we have described a new, simple stereological method of estimating volume tensors in 3D from vertical sections. In contrast to the earlier method, based on observation in several optical planes, see [13], the new method is not sensitive to tissue shrinkage. Furthermore, in the examples considered in the present paper and in earlier simulation studies ([12]), the new estimator is more efficient than the one presented in [13].

Methods of assessing the bias and the precision of the new estimator, based on a bootstrap procedure, have also been provided in the present paper. Note that the estimator of mean particle volume is unbiased, while the estimators of displacement and elongation index may be biased to a degree, depending on the number of sampled particles. In the example, we found that the bias was small and in fact negligible if 100 neurons were sampled. The CVs obtained with 100 neurons were about 5% for volume and elongation while about 15% for displacement.

In a model-based setting, the new method requires that the particle population satisfies the assumption of rotational invariance with respect to the chosen vertical axis. A consequence of rotational invariance, that can be checked with the available observations, is the following. For each particle, consider the profile $X_i \cap (x_i + L)$, generated by the vertical plane centred at the reference point x_i of the particle. Reflect within $x_i + L$ the profile in the vertical axis through x_i. If rotational invariance is satisfied, the distribution of the reflected profiles will be the same as the distribution of the original profiles.

It is part of our future research plans to develop such procedures for checking rotational invariance. In the actual example from BA46, considered in the present paper, we adopted the design-based approach and used a vertical plane that was uniformly rotated around the vertical axis. This approach allowed us to estimate mean particle volume, the displacement in the direction of the vertical axis and the elongation index.

Acknowledgements

The brain studied in the present paper is part of a collection of brains, selected by Karl-Anton Dorph-Petersen and used in a larger brain study under publication. We thank Karl-Anton Dorph-Petersen for fruitful discussions concerning the choice of brain area. We sincerely thank Grazyna Rajkowska for assistance in delineating BA46. We are grateful to Kaj Vedel for the skilful assistance with the graphical illustrations. This work has been supported by Centre for Stochastic Geometry and Advanced Bioimaging, funded by the Villum Foundation.

References

[1] Aizenstein, H.J., Butters, M.A., Wu, M., Mazurkewicz, L.M., Stenger, V.A., Gianaros, P.J., Becker, J.T., Reynolds, C.F. & Carter, C.S. (2009) Altered functioning of the executive control circuit in late-life depression: Episodic and persistent phenomena. *Am. J. Geriat. Psychiat.* **17**, 30–42.

[2] Brown, A.F., Dugina, V., Dunn, G.A. & Vasiliev, J.M. (1989) A quantitative analysis of alterations in the shape of cultured fibroblasts induced by tumour-promoting phorbol ester. *Cell Biol. Int. Rep.* **13**, 357–366.

[3] Dunn, G.A. & Brown, A.F. (1986) Alignment of fibroblasts on grooved surfaces described by a simple geometric transformation. *J. Cell. Sci.* **83**, 313–340.

[4] Dunn, G.A. & Brown, A.F. (1990) Quantifying cellular shape using moment invariants in biological motion. *Lecture Notes in Biomathematics* (ed. by Alt, W. and Hoffman, G.), Springer-Verlag, Berlin, pp. 10–34.

[5] Glantz, L.A. & Lewis, D.A. (2000) Decreased dendritic spine density on prefrontal cortical pyramidal neurons in schizophrenia. *Arch. Gen. Psychiatry* **57**, 65–73.

[6] Guillozet-Bongaarts, A.L., Hyde, T.M., Dalley, R.A., Hawrylycz, M.J., Henry, A., Hof, P.R., Hohmann, J., Jones, A.R., Kuan, C.L., Royall, J., Shen, E., Swanson, B., Zeng, H. & Kleinman, J.E. (2013) Altered gene expression in the dorsolateral prefrontal cortex of individuals with schizophrenia. *Mol. Psychiatr.* **19**, 478–485.

[7] Hadzimichalis, N.M., Previtera, M.L., Moreau, M.P., Li, B., Lee, G.H., Dulencin, A.M., Matteson, P.G., Buyske, S., Millonig, J.H., Brzustowicz, L.M. & Firestein, B.L. (2010) NOS1ap protein levels are altered in BA46 and cerebellum of patients with schizophrenia. *Schizophr. Res.* **124**, 248–250.

[8] Hall, P. (1992) *The Bootstrap and Edgeworth Expansion*. Springer, New York.

[9] Hasselholt, S., Hahn, U., Jensen, E.B.V. & Nyengaard, J.R. (2018) Practical implementation of the planar and spatial rotator in a complex tissue - the brain. *J. Microsc.*, in press. DOI: 10.1111/jmi.12757.

[10] Jensen, E.B.V. & Gundersen, H.J.G. (1993) The rotator. *J. Microsc.* **170**, 35–44.

[11] Koenigs, M. & Grafman, J. (2009) The functional neuroanatomy of depression: Distinct roles for ventromedial and dorsolateral prefrontal cortex. *Behav. Brain Res.* **201**, 239–243.

[12] Kousholt, A., Ziegel, J.F., Kiderlen, M. & Jensen, E.B.V. (2017) Stereological estimation of mean particle volume tensors in $\mathbb{R}^3$ from vertical sections. In *Tensor Valuations and their Applications in Stochastic Geometry and Imaging* (eds. E.B.V. Jensen and M. Kiderlen). *Lecture Notes in Mathematics* **2177**, pp. 423–434. Springer.

[13] Rafati, A.H., Ziegel, J.F., Nyengaard, J.R. & Jensen, E.B.V. (2016) Stereological estimation of particle shape and orientation from volume tensors. *J. Microsc.* **263**, 229–237.

[14] Rajkowska, G. & Goldman-Rakic, P.S. (1995a) Cytoarchitectonic definitions of prefrontal areas of the normal human cortex: I. Remapping of areas 9 and 46 using quantitative criteria. *Cereb. Cortex* **5**, 307–322.

[15] Rajkowska, G. & Goldman-Rakic, P.S. (1995b) Cytoarchitectonic definitions of prefrontal areas of the normal human cortex: II. Variability in locations of areas 9 and 46 and relationship to the Talairach Coordinate System. *Cereb. Cortex* **5**, 323–337.

[16] Selemon, L.D., Rajkowska, G. & Goldman-Rakic, P.S. (1998) Elevated neuronal density in prefrontal area 46 in brains from schizophrenic patients: application of a three-dimensional stereologic counting method. *J. Comp. Neurol.* **392**, 402–412.

[17] Sterio, D.C. (1984) The unbiased estimation of number and size of arbitrary particles using the disector. *J. Microsc.* **134**, 127–136.

[18] Tandrup, T., Gundersen, H.J.G. & Jensen, E.B.V. (1997) The optical rotator. *J. Microsc.* **186**, 108–120.

[19] Zaidel, D.W., Esiri, M.M. & Harrison, P.J. (1997) Size, shape, and orientation of neurons in the left and right hippocampus: Investigation of normal asymmetries and alterations in schizophrenia. *Am. J. Psychiat.* **154**, 812–818.

[20] Ziegel, J.F., Nyengaard, J.R. & Jensen, E.B.V. (2015) Estimating particle orientation and shape using volume tensors. *Scand. J. Stat.* **42**, 813–831.

Appendix A – model-based approach

The particle population of compact particles in $\mathbb{R}^3$ is modelled by a stationary marked point process

$$\{[x_i; X_i - x_i]\},$$

where $x_i \in X_i$ is a reference point of the i'th particle X_i and the mark $X_i - x_i$ is the particle translated such that its reference point is at the origin O.

Let $\mathbf{X}_0$ be a random compact set distributed according to the particle mark distribution. The random set $\mathbf{X}_0$ may be considered as a typical particle with O as its reference point. In this model-based approach, the mean particle volume tensor of rank k is given by $\bar{T}_k = \mathbb{E}T_k(\mathbf{X}_0)$.

The estimator (2) is ratio-unbiased under this model-based approach. To see this, we use that for a function f on compact subsets of $\mathbb{R}^3$

$$\mathbb{E}\sum_{i\in S} f(X_i - x_i) = \mathbb{E}\sum_{x_i\in W} f(X_i - x_i) = \lambda\, V(W)\mathbb{E}f(\mathbf{X}_0),$$

where λ is the intensity of the marked point process. It follows that

$$\frac{\mathbb{E}\sum_{i\in S} f(X_i - x_i)}{\mathbb{E}N(W)} = \mathbb{E}f(\mathbf{X}_0). \tag{8}$$

Choosing f in (8) as the elements of T_k, we get

$$\frac{\mathbb{E}\sum_{i\in S} T_k(X_i - x_i)}{\mathbb{E}N(W)} = \mathbb{E}T_k(\mathbf{X}_0),$$

and the estimator (2) is therefore a ratio-unbiased estimator of $\bar{T}_k = \mathbb{E}T_k(\mathbf{X}_0)$.

The particle process is said to satisfy the *rotational invariance assumption* with respect to a line M through O if the distribution of $\mathbf{X}_0$ is invariant under rotations around M. The line M is called the vertical axis, although M may be an arbitrary line.

It follows from [12, (14.10) with $r = 1, 2$] that, under the rotational invariance assumption, the displacement vector $\bar{c} = \mathbb{E}T_1(\mathbf{X}_0)/\mathbb{E}T_0(\mathbf{X}_0)$ is parallel to the vertical axis and the Miles ellipsoid $\bar{e}$ is a centred ellipsoid of revolution around the vertical axis. In the particular case where the particle process is isotropic, $\bar{c} = O$ and $\bar{e}$ is a ball centred at O with volume equal to the mean particle volume $\bar{v}$.

If we choose a coordinate system such that the vertical plane L is the xy-plane and M is the y-axis, then under the rotational invariance assumption $\mathbb{E}T_k(\mathbf{X}_0)$ can be unbiasedly estimated by $\check{T}_k(\mathbf{X}_0 \cap L)$ where for $k = 0, 1, 2$, cf. [12, (14.10)],

$$\begin{aligned}
\check{T}_0(\mathbf{X}_0 \cap L) &= \pi \int_{\mathbf{X}_0\cap L} |x| \,\mathrm{d}x \,\mathrm{d}y, \\
\check{T}_1(\mathbf{X}_0 \cap L) &= \Big(0, \pi \int_{\mathbf{X}_0\cap L} |x| y \,\mathrm{d}x \,\mathrm{d}y, 0\Big),
\end{aligned}$$

and $\check{T}_2(\mathbf{X}_0 \cap L)$ is a 3×3 diagonal matrix with diagonal elements

$$\check{T}_2(\mathbf{X}_0 \cap L)_{11} = \check{T}_2(\mathbf{X}_0 \cap L)_{33} = \frac{\pi}{4} \int_{\mathbf{X}_0\cap L} |x|^3 \,\mathrm{d}x \,\mathrm{d}y$$

and

$$\check{T}_2(\mathbf{X}_0 \cap L)_{22} = \frac{\pi}{2} \int_{\mathbf{X}_0\cap L} |x| y^2 \,\mathrm{d}x \,\mathrm{d}y.$$

Note that any of these integrals can be determined from information only within $\mathbf{X}_0 \cap L$.

The estimators $\check{T}_k(\mathbf{X}_0 \cap L)$ involve integrals of the form

$$\int_{X\cap L} |x|^{i_1} y^{i_2} \,\mathrm{d}x \,\mathrm{d}y, \tag{9}$$

where X is a compact subset of $\mathbb{R}^3$ and i_1, i_2 are non-negative integers. Note that i_1 is always an odd integer. If the profile $X \cap L$ is not available in digitized form, we may estimate the integral (9), using e.g. a line grid perpendicular to the y-axis. Let $L_1(y)$ denote the line in the xy-plane, perpendicular to the y-axis, at height y. Let y_- and y_+ be the lowest and highest point of the projection of $X \cap L$ onto the

y-axis. Let n be the number of lines, used in the line grid. The set of lines in the line grid is given by

$$L_1(y_j), \qquad j = 0, \ldots, n-1,$$

where $y_j = U + \frac{j}{n}(y_+ - y_-)$ and $U \sim \text{Unif}(y_-, y_- + \frac{y_+ - y_-}{n})$. The integral (9) can then be unbiasedly estimated by

$$\frac{y_+ - y_-}{n} \sum_{j=0}^{n-1} \int_{X \cap L_1(y_j)} |x|^{i_1} \, \mathrm{d}x \times y_j^{i_2}.$$

If $X \cap L_1(y)$ consists of a union of line segments, then for i_1 odd

$$\int_{X \cap L_1(y)} |x|^{i_1} \, \mathrm{d}x = \sum_{P \in \partial X \cap L_1(y)}^{+/-} d(P, M)^{i_1+1}/(i_1 + 1),$$

where $d(P, M)$ is the distance from P to the y-axis, here denoted M, and the convention for the sign of an intersection point is as for the vertical rotator ([10]). More specifically, the intersection points on a given half line are ordered according to decreasing distance to the vertical axis M and are given alternating signs, starting with + for the most distant intersection point. If we in $\check{T}_k(X \cap L)$ use this discretized form instead of (9), we obtain $\widetilde{T}_k(X \cap L)$ in the main text, see (4).

Note that we may increase the efficiency of the estimation procedure by alternately choosing the positive and the negative half line with a random start, as shown in Figure 3 (right) in the main text. In that case, the contribution from each half line should be multiplied by 2 in order to obtain an unbiased estimator of (9).

As mentioned in the main text, rotational invariance may be introduced into the particle model by letting the vertical plane L in (3) be distributed as RL_0, where R is a uniform random rotation around M and L_0 is a fixed vertical plane. The estimator $\widehat{T}_k$ can then be rewritten as

$$\widehat{T}_k = \frac{1}{N(W)} \sum_{i \in S} \widetilde{T}_k(R^{-1}[X_i - x_i] \cap L_0),$$

where R^{-1} is the inverse rotation. So an equivalent description of the situation is that each centred particle $X_i - x_i$ is given a uniform random rotation and then sectioned by the fixed vertical plane L_0.

The induced particle model

$$\{[x(X_i); R^{-1}(X_i - x_i)]\}$$

satisfies the rotational invariance assumption with typical particle $\widetilde{\mathbf{X}}_0 = R^{-1}\mathbf{X}_0$. Using that R is a uniform random rotation around M, we get for any $u \in \mathbb{R}^3$

$$\mathbb{E}R^{-1}u = P_M u,$$

where P_M is the orthogonal projection onto M, and it follows that

$$\mathbb{E}T_1(\widetilde{\mathbf{X}}_0) = P_M \mathbb{E}T_1(\mathbf{X}_0).$$

Since $\mathbb{E}T_0(\widetilde{\mathbf{X}}_0) = \mathbb{E}T_0(\mathbf{X}_0)$, the displacement vector in the induced model is therefore equal to the projection of the displacement vector $\bar{c}$ in the original model onto the vertical axis M. Accordingly, in the design-based approach, $\widehat{T}_1/\widehat{T}_0$ becomes an estimator of $P_M\bar{c}$.

As mentioned earlier, in the design-based approach we may imagine that each centred particle $X_i - x_i$ is given a uniform random rotation around the vertical axis. Remaining shape information is available in the Miles ellipsoid of the induced model. Due to the fact that the induced model satisfies the rotational invariance assumption, this Miles ellipsoid is an ellipsoid of revolution around the vertical axis. The elongation index I is the ratio between the lengths of the semi-axes of this ellipsoid, parallel and perpendicular to the vertical axis.

Appendix B – bootstrap methods

We have data of $r = 5$ repeated measurements for each of $n = 20$ neurons. The overall results (averaging over all 100 measurements) for the data are given in Table 3. We have also used the data to assess the precision of the proposed estimators in the case where a single set of measurements is available for each of $n = 20$ particles. For this situation, Tables 4–6 summarize estimates of the different components of the variance for the volume estimator, the displacement and the elongation index using a bootstrap procedure (and a Taylor expansion approach where possible). For the volume estimator, we also estimated the variances by the empirical counterparts.

The bootstrap procedures work as follows. Let $\mathbf{x} = (x_{kj})_{k=1,\dots,20,j=1,\dots,5}$ be the collection of (vectorized) volume tensors estimated five times for each of $n = 20$ particles from $r = 5$ iid repeated measurements. Our aim is to assess the precision of the estimator of volume, displacement and elongation index in the case when $r = 1$ measurement is available for $n = 20$ particles. For a set $\mathbf{y} = (y_k)_{k=1,\dots,20}$ of one set of measurements per particle, we denote any of these estimators by $\theta(\mathbf{y})$. The overall estimate, averaging over all 100 measurements, is denoted by $\bar{\theta}$. The estimators we consider are not necessarily unbiased, so we aim to assess their bias, variance and coefficient of variation (CV) by a bootstrap procedure. To do so, we draw $B = 10^5$ bootstrap samples, where we first pick a sample $\{k_1, \dots, k_{20}\}$ with replacement from the indices $1, \dots, 20$ and then for each k_i, we pick a random index $j_i \in \{1, \dots, 5\}$. Then, for each bootstrap sample $b = ((k_i, j_i))_{i=1,\dots,20}$, we compute

$$\theta_b^* = \theta((x_{k_i,j_i})_{i=1,\dots,20}).$$

We obtain the following bootstrap estimates of bias and variance

$$\begin{aligned}\widehat{\mathrm{Bias}} &= \frac{1}{B}\sum_b(\theta_b^* - \bar{\theta}) \\ \widehat{\mathrm{Var}} &= \frac{1}{B-1}\sum_b\Big(\theta_b^* - \frac{1}{B}\sum_b\theta_b^*\Big)^2 \end{aligned} \tag{10}$$

where b denotes a bootstrap sample. This procedure was used to obtain the estimates of the total variance in the second last line in Tables 4–6.

The variance of θ can be decomposed as follows

$$\mathrm{Var}\big(\theta(\mathbf{Y})\big) = \mathbb{E}\big(\mathrm{Var}(\theta(\mathbf{Y})|P)\big) + \mathrm{Var}\big(\mathbb{E}(\theta(\mathbf{Y})|P)\big) \tag{11}$$

where $|P$ stands for "given the 20 particles" and $\mathbf{Y}$ is the random variable corresponding to the observation $\mathbf{y}$. We refer to the first part in the above decomposition as the *average design variance* and to the second part as the *particle variance*.

For a bootstrap estimate of the average design variance, we proceed as follows. For $k = 1, \ldots, 20$, we draw a bootstrap observation $j_k \in \{1, \ldots, 5\}$, and then we compute the variance as in (10) using

$$\theta^*_{D,b} = \theta((x_{kj_k})_{k=1,\ldots,20}).$$

We also use a bootstrap procedure to estimate the particle variance. Here, we draw bootstrap samples $b = \{k_1, \ldots, k_n\}$ of size $n = 20$ with replacement from $\{1, \ldots, 20\}$ and use $\theta^*_{P,b}$ to compute the variance as in (10), where

$$\theta^*_{P,b} = \theta\Big(\Big(\frac{1}{5}\sum_{j=1}^{5} x_{k_i j}\Big)_{i=1,\ldots,20}\Big).$$

The bootstrap procedure yields two estimates of the total variance of $\theta(\mathbf{Y})$. One is obtained directly and one is the sum of the two bootstrap estimates of the average design variance and the particle variance. Both estimates agree well overall. The sum is marked with a (+) in Tables 4–6.

For the volume estimators, we can alternatively estimate the total variance and the components of the variance in (11) by the empirical counterparts. For the section estimator used for the displacement, one can alternatively use a Taylor expansion approximation to estimate the variance components. We have

$$\frac{T_1}{T_0} \approx \frac{\mathbb{E}(T_1)}{\mathbb{E}(T_0)} + \frac{1}{\mathbb{E}(T_0)}\big(T_1 - \mathbb{E}(T_1)\big) - \frac{\mathbb{E}(T_1)}{\mathbb{E}(T_0)^2}\big(T_0 - \mathbb{E}(T_0)\big).$$

Hence

$$\begin{aligned}
\mathrm{Var}\left(\frac{T_1}{T_0}\right) &\approx \frac{\mathrm{Var}(T_1)}{\mathbb{E}(T_0)^2} - 2\mathrm{Cov}(T_1, T_0)\frac{\mathbb{E}(T_1)}{\mathbb{E}(T_0)^3} + \mathrm{Var}(T_0)\frac{\mathbb{E}(T_1)^2}{\mathbb{E}(T_0)^4},\\
\mathrm{Var}\left(\frac{T_1}{T_0}\middle| P\right) &\approx \frac{\mathrm{Var}(T_1|P)}{\mathbb{E}(T_0|P)^2} - 2\mathrm{Cov}(T_1, T_0|P)\frac{\mathbb{E}(T_1|P)}{\mathbb{E}(T_0|P)^3}\\
&\quad + \mathrm{Var}(T_0|P)\frac{\mathbb{E}(T_1|P)^2}{\mathbb{E}(T_0|P)^4},\\
\mathrm{Var}\Big(\mathbb{E}\left(\frac{T_1}{T_0}\middle| P\right)\Big) &\approx \frac{\mathrm{Var}(\mathbb{E}(T_1|P))}{\mathbb{E}(T_0)^2} - 2\mathrm{Cov}\big(\mathbb{E}(T_1|P), \mathbb{E}(T_0|P)\big)\frac{\mathbb{E}(T_1)}{\mathbb{E}(T_0)^3}\\
&\quad + \mathrm{Var}(\mathbb{E}(T_0|P))\frac{\mathbb{E}(T_1)^2}{\mathbb{E}(T_0)^4},
\end{aligned}$$

where our data allows us to estimate the quantities on the right hand side of the second and third line by their empirical counterparts. We estimate the total variance as the sum of the average design variance and the particle variance.